Adaptive Sampling Scheduler

Qi Wang ¹, Shuliang Zhu ¹, Jinjia Zhou ¹

¹Department of applied informatics, Hosei University qi.wang.7c@stu.hosei.ac.jp, zhou@hosei.ac.jp

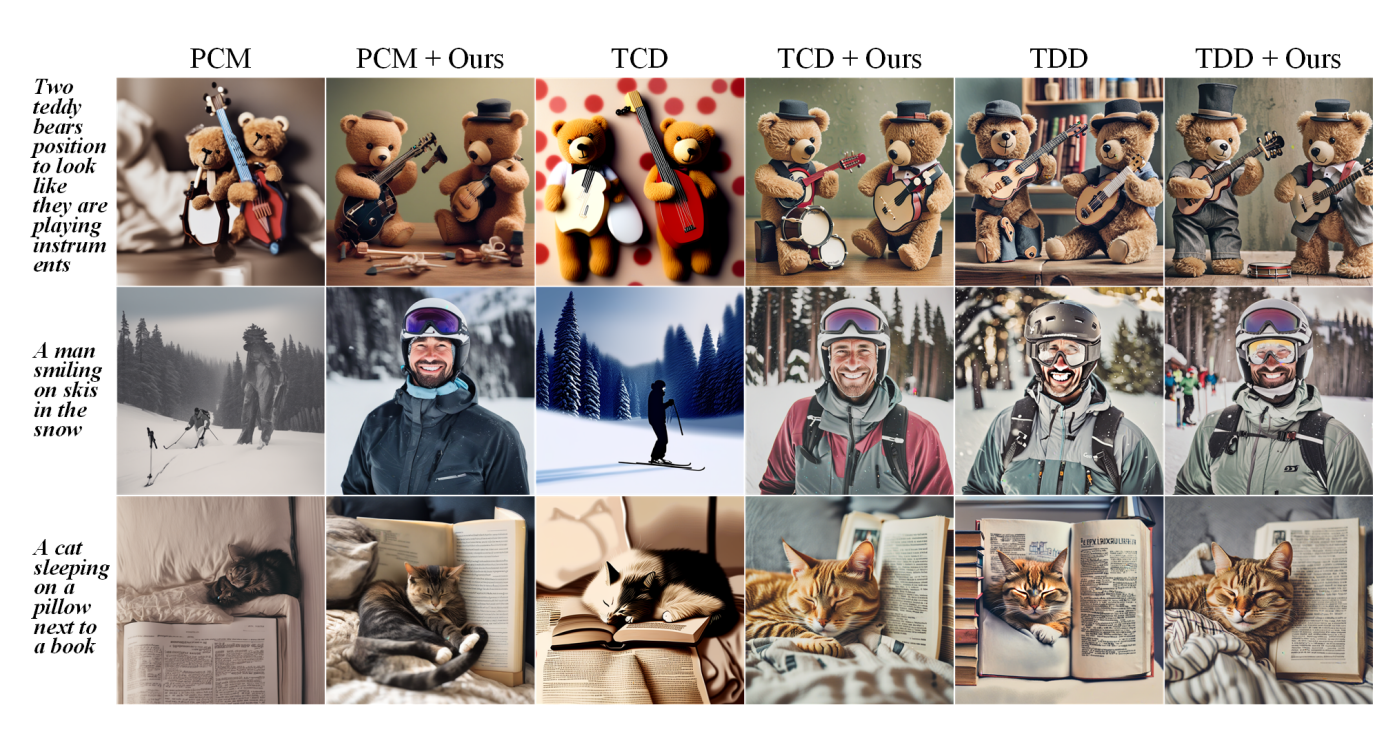


Figure 1: Our method both enhances the structure, details, and color fidelity of generated images and seamlessly adapts to diverse consistency distillation models, unlocking their full practical potential. (All using CFG = 7.5 and 8 steps).

Abstract

Consistent distillation methods have evolved into effective techniques that significantly accelerate the sampling process of diffusion models. Although existing methods have achieved remarkable results, the selection of target timesteps during distillation mainly relies on deterministic or stochastic strategies, which often require sampling schedulers to be designed specifically for different distillation processes. Moreover, this pattern severely limits flexibility, thereby restricting the full sampling potential of diffusion models in practical applications. To overcome these limitations, this paper proposes an adaptive sampling scheduler that is applicable to various consistency distillation frameworks. The scheduler introduces three innovative strategies: (i) dynamic target timestep selection, which adapts to different consistency distillation frameworks by selecting timesteps based on their computed importance; (ii) Optimized alternating sampling along the solution trajectory by guiding forward denoising and backward noise addition based on the proposed time step importance, enabling more effective exploration of the solution space to enhance generation performance; and (iii) Utilization of smoothing clipping and color balancing techniques to achieve stable and high-quality generation results at high guidance scales, thereby expanding the applicability of consistency distillation models in complex generation scenarios. We validated the effectiveness and flexibility of the adaptive sampling scheduler across various consistency distillation methods through comprehensive experimental evaluations. Experimental results consistently demonstrated significant improvements in generative performance, highlighting the strong adaptability achieved by our method.

1 Introduction

Diffusion models (Sohl-Dickstein et al. 2015; Song and Ermon 2019; Ho, Jain, and Abbeel 2020; Song, Meng, and Ermon 2020; Karras et al. 2022a; Rombach et al. 2022a) have achieved state-of-the-art performance in image generation by effectively modeling complex data distributions and supporting sophisticated conditional mechanisms, such as freeform text prompts. Compared to generative adversarial networks (GANs) (Goodfellow et al. 2014; Karras, Laine, and Aila 2019) and variational autoencoders (VAEs) (Kingma, Welling et al. 2013; Sohn, Lee, and Yan 2015), diffusion models employ an iterative denoising procedure that incrementally transforms Gaussian noise into realistic images. Nevertheless, this iterative process typically involves hundreds or thousands of denoising steps, leading to significant computational costs that hinder practical applications.

To overcome these computational limitations, several methods have been proposed to enhance sampling efficiency. These approaches include: (i) accelerating the denoising process by improving ODE solvers (Ho, Jain, and Abbeel 2020; Lu et al. 2022, 2025); (ii) leveraging knowledge distillation techniques (Salimans and Ho 2022; Meng et al. 2023) to condense pretrained diffusion models into fewer-step or even single-step generation networks. Recently, consistency models were introduced by Song et al. (2023) as a promising strategy to accelerate image generation. Subsequently, an increasing number of studies have explored consistency distillation methods (Song et al. 2023; Luo et al. 2023; Kim et al. 2023; Wang et al. 2024; Zheng et al. 2024; Wang et al. 2025), which have proven effective in accelerating generation without compromising image quality. These methods utilize a self-consistency property that regularizes predictions of adjacent timesteps to converge toward the same target timestep. Consistency distillation methods are generally classified into two categories based on the strategy used to select the target timestep: (i) Deterministic-target distillation and (ii) Stochastic-target distillation, as illustrated in Figure 2.

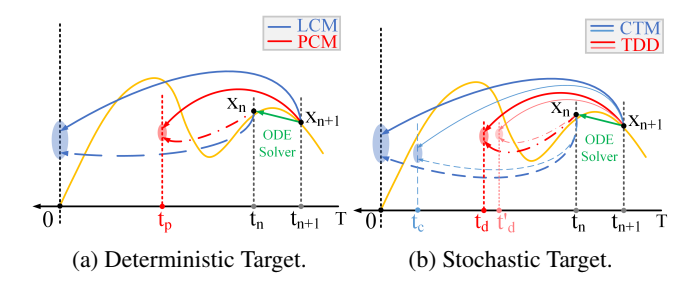


Figure 2: Based on the method of selecting the target timestep, we define existing methods into two categories: (a) Deterministic Target and (b) Stochastic Target.

Deterministic-target distillation employs a fixed mapping pattern to consistently select the same target timestep throughout training, mapping each timestep on the PF-ODE trajectory (Song et al. 2021) to a predetermined target timestep. Early approaches (Song et al. 2023; Luo et al. 2023) predominantly chose the final timestep (0) as the tar-

get, resulting in substantial accumulated errors due to longdistance skip predictions. To mitigate this issue, recent studies (Wang et al. 2024) partition the trajectory into shorter sub-trajectories, using each sub-trajectory's endpoint as the target timestep to reduce the error caused by extensive skip predictions. However, the fixed sub-trajectory lengths limit adaptability to varying inference step counts.

Stochastic-target distillation, conversely, utilizes a one-to-many random mapping strategy, assigning each current timestep to a randomly selected future timestep (Kim et al. 2023; Zheng et al. 2024). This method allows training to generalize across different schedules effectively. Nevertheless, it usually demands significant computational resources. Recent research work (Wang et al. 2025) aims to reduce training overhead by randomly selecting target timesteps from a predefined set, effectively balancing performance and computational efficiency, but the need to set the predefined set in advance limits its generality.

Although these methods have demonstrated promising results, we observed notable limitations stemming from their individualized strategies for selecting target timestep patterns. Specifically, most existing approaches rely on customized sampling schedulers, and their performance substantially deteriorates when applied to general sampling schedulers. Moreover, severe exposure issues arise at higher guidance scale values.

To overcome these shortcomings, we analyzed the diffusion process and identified that the rate of change in the Signal-to-Noise Ratio (SNR) varies distinctly at each timestep along the trajectory. Motivated by this observation, we propose a novel universal Adaptive Sampling Scheduler that leverages the timestep-specific SNR change rate as a criterion for determining the target timestep. This scheduler effectively generalizes across various consistency distillation methods, yielding improved sampling outcomes. Additionally, to mitigate exposure issues at higher guidance scale values, we introduce smoother clipping and color balancing techniques, further enhancing the generation quality.

Main Contributions

- We propose a more reasonable criterion (Importance) for selecting the target timestep based on the rate of change in the signal-to-noise ratio (SNR), combining deterministic-target and stochastic-target.
- We propose an algorithm called Adaptive Sampling Scheduler, which introduces a new target timestep sampling scheduling strategy based on the Importance of timesteps. At the same time, we better mitigate the exposure problem of high guidance scale values through smoothing processing of the sampling process clipping method and color balance method.
- Experiments show that ours provides a more general and reasonable sampling scheme for consistency distillation methods, further improving the performance of the generation task.

2 Related Work

Diffusion models achieve state-of-the-art image generation by iteratively denoising noisy inputs (Sohl-Dickstein et al. 2015; Song and Ermon 2019; Ho, Jain, and Abbeel 2020; Song, Meng, and Ermon 2020; Rombach et al. 2022a), surpassing VAEs and GANs (Kingma, Welling et al. 2013; Sohn, Lee, and Yan 2015; Goodfellow et al. 2014; Karras, Laine, and Aila 2019). However, their multi-step refinement incurs substantial computational cost, hindering deployment in latency-sensitive or real-time applications. This trade-off between fidelity and speed has spurred the search for more efficient sampling paradigms.

In response, Consistency Models (CM) (Song et al. 2023) have emerged as a promising solution. By learning a mapping that projects any point along the diffusion ODE trajectory back to the original data manifold, CMs enable fewor even single-step sampling without degrading image quality. Moreover, they can be trained via knowledge distillation from powerful pretrained diffusion networks or learned independently, offering flexibility across different use cases.

Building on this foundation, numerous consistency distillation methods have been proposed to further optimize efficiency and performance. Latent space CM (LCM) (Luo et al. 2023) employs skip predictions to accelerate generation within latents, while PCM (Wang et al. 2024) partitions the ODE path into sub-trajectories and uses each endpoint as the distillation target. Fixed-target schemes, however, lack adaptability to varying samplers; approaches like CTM (Kim et al. 2023) and TCD (Zheng et al. 2024) introduce random jumps but compromise training efficiency. To strike a better balance, TDD (Wang et al. 2025) selects subtarget timesteps randomly from a predefined set, achieving less training cost.

3 Method

In this section, we will first briefly review diffusion and consistency models and define relevant notations, followed by a detailed description of the concept of **Importance of Timesteps** and **Adaptive Sampling** that we propose.

3.1 Preliminaries

Diffusion Model Diffusion models (Ho, Jain, and Abbeel 2020), or score-based generative models (Song et al. 2021), represent a family of generative models that draw inspiration from the principles of thermodynamics and stochastic processes. These models involve the gradual injection of Gaussian noise into data, followed by the generation of samples from the noise through a process of reverse denoising. Let $p_{data}(x)$ denotes the origin data distribution and $p_t(x)$ is the distribution of x at time t, where $\{x_t|t\in[0,T]\}$. From a continuous-time perspective, the forward process can be described by a stochastic differential equation (SDE) (Song et al. 2021; Lu et al. 2022; Karras et al. 2022b). The stochastic trajectory is described by the following equation:

$$dx_t = f(t)x_t dt + g(t) dw_t, \quad x_0 \sim p_{data}(x_0) \quad (1)$$

$$f(t) = \frac{\mathrm{d}\log\alpha_t}{\mathrm{d}t}, \quad g^2(t) = \frac{\mathrm{d}\sigma_t^2}{\mathrm{d}t} - 2\frac{\mathrm{d}\log\alpha_t}{\mathrm{d}t}\sigma_t^2$$
 (2)

where w_t is the standard Brownian motion, and α_t , σ_t specify the noise schedule. And $f(t)x_t$ denotes the drift coefficient for deterministic changes, and g(t) is the diffusion coefficient for stochastic variations.

The Probabilistic Flow Ordinary Differential Equation (PF-ODE) (Song et al. 2021; Lu et al. 2022) proposes that diffusion processes described by stochastic differential equations (SDE) can be described in deterministic form using deterministic processes with the same marginal distribution. The PF-ODE is formulated as:

$$dx_t = \left[f(t)x_t - \frac{1}{2}g(t)^2 \nabla_x \log p_t(x) \right] dt$$
 (3)

where $\nabla_x \log p_t(x)$ is called the *score function*, indicates the gradient of the log density of $p_t(x)$. Empirically, in the standard diffusion training process, we aim to train a score model $s_\phi(x,t)$ to approximate this score function using by score matching, which is equivalent to $s_\phi(x,t) \approx \nabla_x \log P_t(x) = \mathbb{E}_{x_0 \sim P(x_0|x)} \left[\nabla_x \log P_t(x|x_0) \right]$, substitue the $\nabla_x \log P_t(x)$ with $s_\phi(x,t)$, and we get the empirical PFODE. Despite the plethora of methods such as (Song, Meng, and Ermon 2020; Lu et al. 2022; Karras et al. 2022b) can approximate ODE solutions, using only a handful of sampling steps (e.g., 4 or 8) inevitably incurs significant discretization errors, leading to unsatisfactory outcomes.

Consistency Models CM (Song et al. 2023) constitutes a novel family of generative models capable of one-step or few-step generation by learning a mapping that projects any intermediate points along the PF-ODE trajectory back to the initial point. A consistency model $f_{\theta}(\cdot,t)$ learns to achieve $f_{\theta}(x_t,t)=x_{\epsilon}$ must adhere to the *self-consistency property*:

$$f_{\theta}(x_t, t) = f_{\theta}(x_{t'}, t'), \quad \forall t, t' \in [\epsilon, T]$$
 (4)

where ϵ is a fixed small positive number. CM can be trained using pre-trained model distillation or trained from scratch, with the former referred to as consistency distillation.

Consistency Distillation For uniformity in subsequent notation, we define ϕ to denote the teacher model, f_{θ} to denote the student consistency model, and Φ to denote the selected numerical ODE Solver, and the $\hat{x}_{t_n}^{\phi}$ is one-step estimation of x_{t_n} from $x_{t_{n+1}}$ by Φ as follows:

$$\hat{x}_{t_n}^{\phi} \leftarrow x_{t_{n+1}} + (t_n - t_{n+1})\Phi(x_{t_{n+1}}, t_{n+1}; \phi)$$
 (5)

To enforce the *self-consistency property*, define the consistency loss as follows:

$$\mathcal{L}_{cm} = \mathbb{E}_{x,t} \left[d(f_{\theta}(x_{t_{n+1}}, t_{n+1}, \tau), f_{\theta^{-}}(\hat{x}_{t_n}^{\phi}, t_n, \tau)) \right]$$
 (6)

where d(.,.) is a chosen metric function to calculate the distance between two samples, e.g., the squared ℓ_2 distance. The f_{θ^-} is the consistency model with a target model updated with exponential moving average (EMA) of the parameter f_{θ} we intend to learn, here $\theta^- \leftarrow \mu \theta^- + (1-\mu)\theta$, $\mu=0.95$, and the τ refers to the target timestep.

For existing work, deterministic-target distillation method CM (Song et al. 2023) set $\tau=0$ for any timestep t_{n+1} , and LCM (Luo et al. 2023) set $\tau=t_n$ to achieve the skip prediction, drastically reducing the length of time schedule from

thousands to dozens. Next, PCM (Wang et al. 2024) divide the entire trajectory into multiple phased sub-trajectories (e.g. 4, 8), select the next phased ending point to be τ . For stochastic-target distillation methods, CTM (Kim et al. 2023) selects a random τ within the interval $[0,t_n]$, and TDD (Wang et al. 2025) selects a random $\tau \in [(1-\eta)\ t_m,t_m]$ where $t_m \in [t-e,t]$, t is a predefined subset timesteps, the e,η are preset hyper-parameters.

We found that previous studies either used a fixed target timestep or a random target timestep. They lacked an criterion for selecting the target timestep. Therefore, we considered *How to more reasonably select the target timestep in a* standardized manner?

3.2 Importance of Timesteps



Figure 3: Forward diffusion results at each timestep by DDPM (Ho, Jain, and Abbeel 2020).

For the sake of this concern, we first review the forward diffusion process illustrated in Figure 3. The visualization makes it clear that, up to T=200, the image content remains almost fully discernible, while beyond T=800 it becomes virtually unrecognizable. In these two regions, the signal retention rates are respectively very high and very low, and the visual changes from step to step are minimal. In contrast, during the intermediate phase ($T=400 \rightarrow 700$), the images undergo the most significant transformations, reflecting a rapid degradation of detail. Therefore, we further defined the rate of signal change using Equation (7). We call it "Importance (I)". We calculated the importance of all time steps, and the visualization results are shown in Figure 4.

$$I_{t} = \frac{\left|\nabla_{t} \ln\left(\frac{\overline{\alpha}_{t}}{1 - \overline{\alpha}_{t}} + \varepsilon\right)\right|^{-1}}{\max_{0 \leq j < T} \left|\nabla_{j} \ln\left(\frac{\overline{\alpha}_{j}}{1 - \overline{\alpha}_{j}} + \varepsilon\right)\right|^{-1}}, \bar{\alpha}_{t} = \prod_{i=1}^{t} \alpha_{i} \quad (7)$$

The $\varepsilon=1e^{-8}$ to avoid division by zero. As can be seen in Figure 4, the changes in the diffusion process shown in Figure 3 can be reasonably approximated by Equation (7) (I more closer to 1, the faster the change; more closer to 0, the slower the change).

Through analysis of the diffusion process, we argue that when selecting the target timestep, *not all timesteps should* be treated equally, but rather should depend on the importance of the current timestep. Therefore, based on this finding, we proposed Adaptive Sampling.

3.3 Adaptive Sampling

In previous studies (Song et al. 2023; Luo et al. 2023; Wang et al. 2024), most work has used equidistant sampling. The TDD (Wang et al. 2025) mentions that extending the sampling method to non-equidistant sampling will yield better

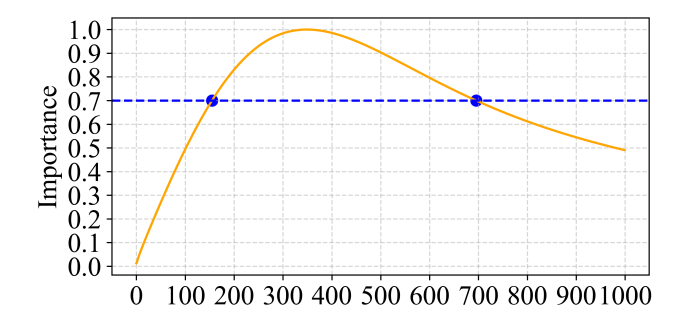


Figure 4: The corresponding importance of each timestep during the diffusion process.

sampling results, but it uses predefined timesteps for sampling. In order to address these limitations, thus, we propose Adaptive Sampling.

According to Equation 7, we calculate the importance corresponding to all timesteps. We take the timestep with the maximum importance in different intervals as the importance sampling timestep T_I . At the same time, we define the original equidistant sampling timestep T_E . The equation is defined as follows:

$$T_{as} = \{t_i \mid t_i \in T_I, I_t > \theta\} \cup \{t_i \mid t_i \in T_E, I_t \le \theta\}$$
 (8)

and according to Figure 3 and Figure 4, we set $\theta=0.7$ as the threshold. For a more intuitive understanding, we illustrate the process in Figure (5a). Here, we finally obtain a set of target timesteps for T_{as} , in which the number of target timesteps is still the same as T_n , but the intervals between adjacent target timesteps are not the original equal intervals, but have changed.

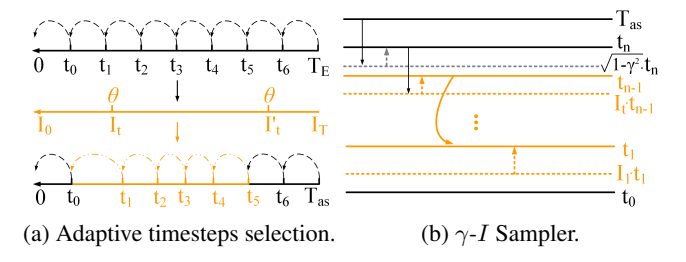


Figure 5: The adaptive sampling process that we propose.

In addition, we referred to the γ sampler proposed in (Kim et al. 2023), which solves x_0 by alternately performing forward and backward jumps on the solution trajectory. The γ parameter can be adjusted to control the proportion of randomness (default $\gamma=0.2$), which has been proven to improve the generation quality to a certain extent. On this basis, we optimized using importance and replaced the forward and backward jumps based on Equation 8, γ -I Sampler, as shown in Figure (5b). Here, our method can be easily understood from the figure (5b). The γ -I sampler first denoise the current noise sample using the network in each backward, and then reintroduces noise proportionally. The denoising

Methods	FID ↓			CLIP Score ↑			Inception Score ↑		
	2 steps	4 steps	8 steps	2 steps	4 steps	8 steps	2 steps	4 steps	8 steps
PCM (Wang et al. 2024)	372.82	112.65	31.73	18.44	24.18	30.44	1.71	11.67	25.78
PCM + Ours	65.83	29.40	23.21	30.22	30.40	31.52	16.54	24.59	31.80
TCD (Zheng et al. 2024)	363.50	103.66	53.72	18.73	26.05	30.44	1.82	12.47	17.83
TCD + Ours	62.89	28.51	27.44	28.88	31.71	32.06	16.33	28.02	32.17
TDD (Wang et al. 2025)	58.45	29.80	27.72	29.27	31.12	31.47	17.18	27.02	29.72
TDD + Ours	55.71	27.88	26.60	29.49	31.47	31.74	17.62	29.36	32.88
Δ (MPI)	203.45	53.44	11.97	7.38	4.08	0.99	9.93	10.27	7.84

Table 1: Performance comparison at 1024×1024 resolution using Stable Diffusion XL (Podell et al. 2023), evaluated on FID (lower is better), CLIP Score, and Inception Score (higher is better), with 2, 4, and 8 sampling steps. The Δ denotes Mean Performance Improvement (MPI).

Methods	FID ↓			CLIP Score ↑			Inception Score ↑		
	2 steps	4 steps	8 steps	2 steps	4 steps	8 steps	2 steps	4 steps	8 steps
LCM (Luo et al. 2023)	86.33	88.20	109.84	28.02	26.48	25.19	14.28	11.73	8.71
LCM + Ours	58.01	30.04	47.67	30.18	30.71	30.79	17.18	28.81	19.84
PCM (Wang et al. 2024)	424.04	89.99	38.82	18.99	26.51	30.02	1.76	12.49	21.07
PCM + Ours	60.66	23.11	22.47	29.93	30.37	31.03	16.86	28.93	31.65
Δ (MPI)	195.85	62.52	39.26	6.55	4.05	3.31	9.00	16.76	10.86

Table 2: Performance comparison at 512 × 512 resolution using Stable Diffusion v1-5 (Rombach et al. 2022b).

and noise addition process is as follows:

$$t_{n+1} \xrightarrow{\text{Denoise}} \sqrt{(1-\gamma)^2} * t_n \xrightarrow{\text{Noisify}} t_n, t_n \in T_E \quad (9)$$

$$t_n \xrightarrow{\text{Denoise}} I_t * t_{n-1} \xrightarrow{\text{Noisify}} t_{n-1}, t_{n-1} \in T_I \quad (10)$$

In addition, in all previous methods, when high classifier-free guidance (CFG) (Ho and Salimans 2022) scaling was used, there were varying degrees of exposure issues. To alleviate this issue, we consulted the solutions offered by (Saharia et al. 2022; Lu et al. 2022). We then integrated these solutions into our sampling scheduler after our optimization, which effectively alleviated the exposure issue. Additionally, we implemented a color balance method to assist in generating higher guidance scales. The formula is as follows:

$$x_0 = \frac{e^{x_0} - e^{-x_0}}{e^{x_0} + e^{-x_0}} \tag{11}$$

$$x_c = x_c - \alpha \cdot \text{mean}(x_c), \ x_0 = x_0 - \beta \cdot \text{mean}(x)$$
 (12)

where x_c is the each channel of x_0 , the $\alpha, \beta = 0.5$. Without changing the shape of x_0 , we used the hyperbolic tangent function to map all values to the range (-1,1), thereby removing outliers. Compared to the mapping methods in (Saharia et al. 2022; Lu et al. 2022), this method does not require prior deformation and provides a more direct and smooth mapping. Although hyperbolic tangent function compresses values between (-1,1), if the x_0 deviates too much from 0 (e.g. exposure situation), most values will fall into the saturation zone (output tends to ± 1). Therefore, we further offset the mean of x_0 within the channel and across

the entire image by a certain proportion, so that more values are concentrated in the linear interval of hyperbolic tangent function, thereby retaining more effective information.

4 Experiments

4.1 Backbones

We chose text-to-image generation as the basic task for all experimental evaluations. For an objective and comprehensive comparison, we conducted image generation experiments at 1024 resolution and 512 resolution, selecting two different architectures as the backbone for the comparison experiments: Stable Diffusion XL (SDXL) (Podell et al. 2023) for 1024 resolution and Stable Diffusion v1-5 (SD v1-5) (Rombach et al. 2022b) for 512 resolution.

4.2 Baselines & Evaluation

We choose previous research: LCM (Luo et al. 2023), PCM (Wang et al. 2024), TCD (Zheng et al. 2024) and TDD (Wang et al. 2025) as baselines. All relevant backbone models and baseline models have been open-sourced. The PCM, TCD, TDD are used to generate the resolution of 1024, while LCM, PCM are also used to generate 512 resolution. For performance evaluation, we utilize the validation split of the MS COCO 2014 dataset (Lin et al. 2014), following Karpathy's 30K partition, and to generate image prompts we use the first sentence of each image's default caption. And, for different resolutions of different backbones, we report the key metrics of the generated images, adopt three different metrics to assess our model's outputs: the Fréchet Inception Distance (FID) (Heusel et al. 2017) to measure the



Figure 6: Qualitative comparison of different methods using 2, 4, and 8 steps for two diffusion models (SD V1-5, SDXL).

distributional similarity between generated and real images, the CLIP Score (Radford et al. 2021) to quantify semantic alignment with input prompts, and the Inception Score (IS) (Salimans et al. 2016) to evaluate both the visual quality and diversity of the generated samples.

4.3 Main Results

The quantitative results in Table 1 and Table 2 demonstrate that our method consistently outperforms the baseline method across both SDXL and SD v1-5. Notably, there are significant performance gains in the smaller step (e.g. 2 or 4), highlighting the efficiency and superiority of our approach.

As can be seen from Table 2, the LCM (Luo et al. 2023) showed a counterintuitive experimental phenomenon at 4 steps and 8 steps. When the number of steps was larger, the FID and IS evaluations showed a decline. Through experimentation, we found that this is because in the original LCM method, distillation is performed using relatively large CFG values during training, so when large CFG values are used in inference, the more steps there are, the more serious the exposure issue becomes. Therefore, this situation occurs, but of course, our method can still greatly alleviate this issue.

From a qualitative standpoint, Figure 6 vividly illustrates our method's prowess under extreme sampling constraints (2 or 4 steps, CFG = 7.5): whereas the SDXL and SD v1-

5 baselines produce nothing more than chaotic noise and meaningless textures, our approach consistently reconstructs coherent, high-fidelity images even with only two steps.

Quantitatively, Table 1 confirms this advantage, with baseline FID scores skyrocketing into the hundreds at 2 or 4 steps, whereas our scheduler brings FID down to practical levels across 2, 4 steps, demonstrating both the robustness and superiority of our method in low-budget sampling scenarios.

4.4 Ablation Study

In order to gain a more comprehensive understanding of our approach, we conducted a series of detailed ablation experiments on the methods proposed in our paper.

Different Importance Values This paper proposes a method for selecting the target timestep based on the importance I in Equation 7. In order to verify the effect of different importance thresholds θ on the overall generation results, we selected different values of θ and conducted further comparative experiments. We selected six different values, $\theta=0$, 0.6, 0.7, 0.8, 0.9 and 1, for the experiment. As shown in Figure 7, we can see that when $\theta=0$, timesteps are chosen purely by their importance, yielding images that are more random yet still retain their overall structure. When $\theta=0.6$, some randomness still exists (e.g. multiple glasses, distorted bottle structure). In contrast, when $\theta=1$, sampling proceeds



Figure 7: The first row from left to right is $\theta = 0$, 0.6, 0.7; the second row from left to right is $\theta = 0.8$, 0.9, 1. Prompt: A pizza and grapes sit on a tray next to a drink.

at fixed intervals, this produces outputs that more faithfully follow the prompt but introduces structural ambiguity (e.g., the wine glass and grapes appear to merge), still exists in $\theta=0.9$. When $\theta=0.7$ or $\theta=0.8$, the image structure is clear and consistent with the prompt, and when $\theta=0.8$ the font on the bottle is clearer and the colors are richer. This is consistent with the importance curve shown in Figure 4, further proving that the importance we propose is reasonable and effective.

The γ -I Sampler To more clearly highlight the effectiveness of the γ -I sampler we propose, we compare it with the original γ sampler proposed by CTM (Kim et al. 2023) and one that does not use the γ sampler (only the denoising process, without adding noise) (all other parameters are the same except for the sampler). The results in Figure 8 show



Figure 8: Prompt: *Small monkey eating fruit sitting on a rock.* CFG = 7.5 and 8 steps.

that without using the γ sampler, the generated structure is the worst (e.g., with three paws and two tails). Using the γ sampler improves the situation, and when using our proposed γ -I sampler, the structure is the most reasonable, the actions are more consistent with the prompt (eating fruit) and more details in fruits.

Smooth clipping and color balance In order to verify the effectiveness of the proposed smoothing clipping and color balancing techniques, all parameters of the other methods proposed in this paper were fixed and compared with

the previous clipping methods. The experimental results are



Figure 9: The first row w/o our method, using the clipping method same with (Saharia et al. 2022; Lu et al. 2022), and the second row w/ our method. We circled some obvious areas in the picture. All results are obtained by using CFG = 7.5 and 8 steps.

presented in Figure 9. Our approach markedly alleviates color overexposure, yielding cleaner and more natural images. Previous consistency distillation methods often suffered from pronounced overexposure caused by classifier-free guidance (CFG) scaling during distillation. Consequently, these methods typically resorted to low guidance scales (e.g., CFG = 1 or 2) at sampling. By incorporating the strategies of (Saharia et al. 2022; Lu et al. 2022), we refined their clipping procedures and introduced a dedicated colorbalancing step, which significantly suppresses overexposure artifacts and improves overall color fidelity. A detailed discussion of the issue of exposure to high CFG values is provided in the Appendix.

5 Conclusion

We introduce a novel, universally applicable adaptive sampling scheduler grounded in consistency distillation, designed to overcome the key limitations of previous deterministic or stochastic target strategies. By dynamically selecting target timesteps based on their computed importance, quantified via the rate of change in signal-to-noise ratio (SNR), our scheduler adaptively focuses computation on the most critical diffusion steps, meanwhile, we further optimize the alternating forward and backward jumps according to timestep importance, substantially enhancing generation quality across diverse consistency distillation methods. And, employ a combination of smoothing clipping and color balancing to further mitigate exposure artifacts at high guidance scales. Extensive experiments on standard SDXL and SD v1-5 benchmarks at multiple resolutions confirm the effectiveness and robustness of our method. Moreover, our scheduler can seamlessly integrates with existing consistency distillation frameworks, further underscoring its practicality. We hope these insights will propel further advances in fast, high-quality generative sampling.

References

Goodfellow, I. J.; Pouget-Abadie, J.; Mirza, M.; Xu, B.; Warde-Farley, D.; Ozair, S.; Courville, A.; and Bengio, Y.

- 2014. Generative adversarial nets. Advances in neural information processing systems, 27.
- Heusel, M.; Ramsauer, H.; Unterthiner, T.; Nessler, B.; and Hochreiter, S. 2017. Gans trained by a two time-scale update rule converge to a local nash equilibrium. *Advances in neural information processing systems*, 30.
- Ho, J.; Jain, A.; and Abbeel, P. 2020. Denoising diffusion probabilistic models. *Advances in neural information processing systems*, 33: 6840–6851.
- Ho, J.; and Salimans, T. 2022. Classifier-free diffusion guidance. *arXiv preprint arXiv:2207.12598*.
- Karras, T.; Aittala, M.; Aila, T.; and Laine, S. 2022a. Elucidating the design space of diffusion-based generative models. *Advances in neural information processing systems*, 35: 26565–26577.
- Karras, T.; Aittala, M.; Aila, T.; and Laine, S. 2022b. Elucidating the design space of diffusion-based generative models. *Advances in neural information processing systems*, 35: 26565–26577.
- Karras, T.; Laine, S.; and Aila, T. 2019. A style-based generator architecture for generative adversarial networks. In *Proceedings of the IEEE/CVF conference on computer vision and pattern recognition*, 4401–4410.
- Kim, D.; Lai, C.-H.; Liao, W.-H.; Murata, N.; Takida, Y.; Uesaka, T.; He, Y.; Mitsufuji, Y.; and Ermon, S. 2023. Consistency Trajectory Models: Learning Probability Flow ODE Trajectory of Diffusion. *arXiv* preprint arXiv:2310.02279.
- Kingma, D. P.; Welling, M.; et al. 2013. Auto-encoding variational bayes.
- Lin, T.-Y.; Maire, M.; Belongie, S.; Hays, J.; Perona, P.; Ramanan, D.; Dollár, P.; and Zitnick, C. L. 2014. Microsoft coco: Common objects in context. In *European conference on computer vision*, 740–755. Springer.
- Lu, C.; Zhou, Y.; Bao, F.; Chen, J.; Li, C.; and Zhu, J. 2022. Dpm-solver: A fast ode solver for diffusion probabilistic model sampling in around 10 steps. *Advances in neural information processing systems*, 35: 5775–5787.
- Lu, C.; Zhou, Y.; Bao, F.; Chen, J.; Li, C.; and Zhu, J. 2025. Dpm-solver++: Fast solver for guided sampling of diffusion probabilistic models. *Machine Intelligence Research*, 1–22.
- Luo, S.; Tan, Y.; Huang, L.; Li, J.; and Zhao, H. 2023. Latent Consistency Models: Synthesizing High-Resolution Images with Few-Step Inference. arXiv:2310.04378.
- Meng, C.; Rombach, R.; Gao, R.; Kingma, D.; Ermon, S.; Ho, J.; and Salimans, T. 2023. On distillation of guided diffusion models. In *Proceedings of the IEEE/CVF conference on computer vision and pattern recognition*, 14297–14306.
- Podell, D.; English, Z.; Lacey, K.; Blattmann, A.; Dockhorn, T.; Müller, J.; Penna, J.; and Rombach, R. 2023. Sdxl: Improving latent diffusion models for high-resolution image synthesis. *arXiv preprint arXiv:2307.01952*.
- Radford, A.; Kim, J. W.; Hallacy, C.; Ramesh, A.; Goh, G.; Agarwal, S.; Sastry, G.; Askell, A.; Mishkin, P.; Clark, J.; et al. 2021. Learning transferable visual models from natural language supervision. In *International conference on machine learning*, 8748–8763. PmLR.

- Rombach, R.; Blattmann, A.; Lorenz, D.; Esser, P.; and Ommer, B. 2022a. High-resolution image synthesis with latent diffusion models. In *Proceedings of the IEEE/CVF conference on computer vision and pattern recognition*, 10684–10695.
- Rombach, R.; Blattmann, A.; Lorenz, D.; Esser, P.; and Ommer, B. 2022b. High-resolution image synthesis with latent diffusion models. In *Proceedings of the IEEE/CVF conference on computer vision and pattern recognition*, 10684–10695.
- Saharia, C.; Chan, W.; Saxena, S.; Li, L.; Whang, J.; Denton, E. L.; Ghasemipour, K.; Gontijo Lopes, R.; Karagol Ayan, B.; Salimans, T.; et al. 2022. Photorealistic text-to-image diffusion models with deep language understanding. *Advances in neural information processing systems*, 35: 36479–36494.
- Salimans, T.; Goodfellow, I.; Zaremba, W.; Cheung, V.; Radford, A.; and Chen, X. 2016. Improved techniques for training gans. *Advances in neural information processing systems*, 29.
- Salimans, T.; and Ho, J. 2022. Progressive distillation for fast sampling of diffusion models. *arXiv preprint arXiv:2202.00512*.
- Sohl-Dickstein, J.; Weiss, E.; Maheswaranathan, N.; and Ganguli, S. 2015. Deep unsupervised learning using nonequilibrium thermodynamics. In *International conference on machine learning*, 2256–2265. pmlr.
- Sohn, K.; Lee, H.; and Yan, X. 2015. Learning structured output representation using deep conditional generative models. *Advances in neural information processing systems*, 28.
- Song, J.; Meng, C.; and Ermon, S. 2020. Denoising diffusion implicit models. *arXiv preprint arXiv:2010.02502*.
- Song, Y.; Dhariwal, P.; Chen, M.; and Sutskever, I. 2023. Consistency Models. *arXiv preprint arXiv:2303.01469*.
- Song, Y.; and Ermon, S. 2019. Generative modeling by estimating gradients of the data distribution. *Advances in neural information processing systems*, 32.
- Song, Y.; Sohl-Dickstein, J.; Kingma, D. P.; Kumar, A.; Ermon, S.; and Poole, B. 2021. Score-Based Generative Modeling through Stochastic Differential Equations. In *International Conference on Learning Representations*.
- Wang, C.; Guo, Z.; Duan, Y.; Li, H.; Chen, N.; Tang, X.; and Hu, Y. 2025. Target-driven distillation: Consistency distillation with target timestep selection and decoupled guidance. In *Proceedings of the AAAI Conference on Artificial Intelligence*, volume 39, 7619–7627.
- Wang, F.-Y.; Huang, Z.; Bergman, A.; Shen, D.; Gao, P.; Lingelbach, M.; Sun, K.; Bian, W.; Song, G.; Liu, Y.; et al. 2024. Phased consistency models. *Advances in neural information processing systems*, 37: 83951–84009.
- Zheng, J.; Hu, M.; Fan, Z.; Wang, C.; Ding, C.; Tao, D.; and Cham, T.-J. 2024. Trajectory Consistency Distillation. arXiv:2402.19159.

A Appendix

A.1 Exposure Problem Analysis

In text-conditioned diffusion, a neural network ϵ_{ϕ} is trained to predict the noise at each timestep t given a noisy x_t and a positive prompt embedding c. By also training with c replaced by the null embedding \varnothing , the model acquires an unconditional predictor $\epsilon_{\phi}(x_t,t,\varnothing)$. At inference, Classifier-Free Guidance (Ho and Salimans 2022) interpolates these two estimates using a guidance scale $\omega > 0$:

$$\tilde{\epsilon}_{\phi}(x_t, t, c; \omega) = (1 + \omega) \, \epsilon_{\phi}(x_t, t, c) - \omega \, \epsilon_{\phi}(x_t, t, \varnothing) \tag{13}$$

where $\omega=0$ yields pure conditional sampling and larger ω amplifies the conditional signal. This simple mechanism requires no auxiliary classifier, affords a smooth fidelity-diversity trade-off via ω , and has been instrumental in models such as Stable Diffusion (Rombach et al. 2022a), Imagen (Saharia et al. 2022).

Define $\epsilon_{\theta}(x_t,t,c)$ as a consistency model is trained to match the ODE trajectory in a single or few steps. Naively solving the diffusion ODE with pure conditional predictions $\epsilon_{\theta}(x_t,t,c)$ leads to trajectories that deviate from the data manifold, yielding blurred or structurally inconsistent outputs. Hence, each step employs a CFG-augmented estimate that may also incorporate a null or negative embedding c_n :

$$\epsilon_{\theta}(x_t, t, c, c_n; \omega) = \epsilon_{\theta}(x_t, t, c_n) + \omega \left(\epsilon_{\theta}(x_t, t, c) - \epsilon_{\theta}(x_t, t, c_n)\right)$$
(14)

At inference, if we further apply CFG with scale ω' to the consistency model itself. Denoting by $x_t^{\omega'}$ the state distilled under diversity scale ω' , its noise prediction becomes:

$$\hat{\epsilon} = (1 + \omega) \,\epsilon_{\theta} (x_{t}^{\omega'}, t, c) - \omega \,\epsilon_{\theta} (x_{t}^{\omega'}, t, \varnothing) \tag{15}$$

As theoretical analysis in (Wang et al. 2024) shows that this compounds the consistency model: for all $t' \leq t$, we have:

$$\epsilon_{\theta}(x_{t}, t, c, c_{n}; \omega') \propto \omega \omega' \left(\epsilon_{\phi}(x_{t'}, t', c) - \epsilon_{m}^{\phi}\right) + \epsilon_{\phi}(x_{t'}, t', c_{n})$$
(16)

$$+ \epsilon_{\phi}(x_{t'}, t, c_{n})$$
where $\epsilon_{m}^{\phi} = (1 - \alpha) \epsilon_{\phi}(x_{t'}, t', c_{n}) + \alpha \epsilon_{\phi}(x_{t'}, t', \varnothing)$ and $\alpha = (\omega - 1)/(\omega \omega')$.
This is equivalent to scaling the predictions of the origin

This is equivalent to scaling the predictions of the original diffusion model by a factor of ω ω' , which leads to severe exposure issues when using larger CFG values during inference. Thus, large CFG (e.g., CFG > 7) accentuates edges and contrast but suppresses texture complexity and flattens fine details, whereas setting CFG (e.g., CFG = 1) too low causes the ODE path to drift off-manifold, producing blurry or semantically inconsistent samples.

In addition, we observe that prior work has typically proposed its own solutions. For example, PCM (Wang et al. 2024) trains and stores model weights for various values of ω to accommodate subsequent applications with different ω' for inference; TCD (Zheng et al. 2024) provides weights that perform well when CFG is around 2.5 but, as our experiments show in Table 1 and Figure 6, degrade severely when CFG > 7; and TD (Wang et al. 2025) mitigates the exposure

problem by fixing CFG at 3.5 during training, and using the clipping method proposed by (Saharia et al. 2022; Lu et al. 2022), yet the exposure issue still occurs when CFG (e.g. 7.5) is higher or when the number of inference steps is increased (e.g. to 8 steps).

In practice, most diffusion models employ a CFG scale of 7.5 to achieve outputs that adhere more closely to the prompt. Therefore, we did not deliberately choose a smaller CFG value; instead, to remain consistent with real-world usage, all of our experiments were conducted with CFG set to 7.5. Using our method, the severe overexposure issues induced by large CFG values (i.e. CFG > 7) can be effectively mitigated.

A.2 Smooth clipping & color balance

When employing a high CFG scale (e.g. $\omega=7.5$) together with more inference steps (8 steps), most existing methods exhibit severe over-exposure artifacts. Even applying the cropping strategy of prior work (Saharia et al. 2022; Lu et al. 2022) only partially mitigates the effect-the exposure problem persists.

In an over-exposed image, the vast majority of pixel magnitudes cluster near the maximum, so the quantile-based threshold:

$$s = \text{Clamp (quantile}_{\alpha}(|x|), 1, V)$$
 (17)

(with, e.g., $\alpha=0.995$) almost always saturates at its upper bound V. All Pixels are then normalized via follow:

$$\tilde{x}_i = \frac{\text{clip}(x_i, -s, s)}{s} \tag{18}$$

which, when s=V, reduces to $\tilde{x}_i=\frac{x_i}{V}$. Under this mapping, even mid-tone values (e.g. $x_i\approx 0.5V$) are confined to the narrow interval [0.5,1], collapsing the dynamic range, obliterating contrast, and flattening image details.

By contrast, our proposed $\tanh(x)$ and color balance scheme overcomes these issues in two ways. First, $\tanh(x)$ enforces soft saturation it smoothly compresses all values into (-1,1) and only gradually attenuates extremes, rather than hard-clipping them. This preserves continuous saturation transitions and avoids abrupt clipping artifacts. Second, if the x_0 deviates too much from reasonable area (e.g. exposure situation), most values will fall into the saturation zone (output tends to ± 1) as clamp in (Saharia et al. 2022; Lu et al. 2022), so continue subtracting the per-channel and then the global mean recenter the data around reasonable area, maintaining relative brightness differences across regions without uniformly suppressing low-level and mid-level intensities through a single global threshold.

A.3 More experimental results

To further demonstrate the effectiveness and robustness of our method, we have added additional visual comparisons in Figure 10. Here, we select the original form of the methods that performed better, PCM (Wang et al. 2024) and TDD (Wang et al. 2025), and combined them with our method to clearly highlight the improvements of our solution in terms of detail preservation, exposure correction, and overall visual fidelity.

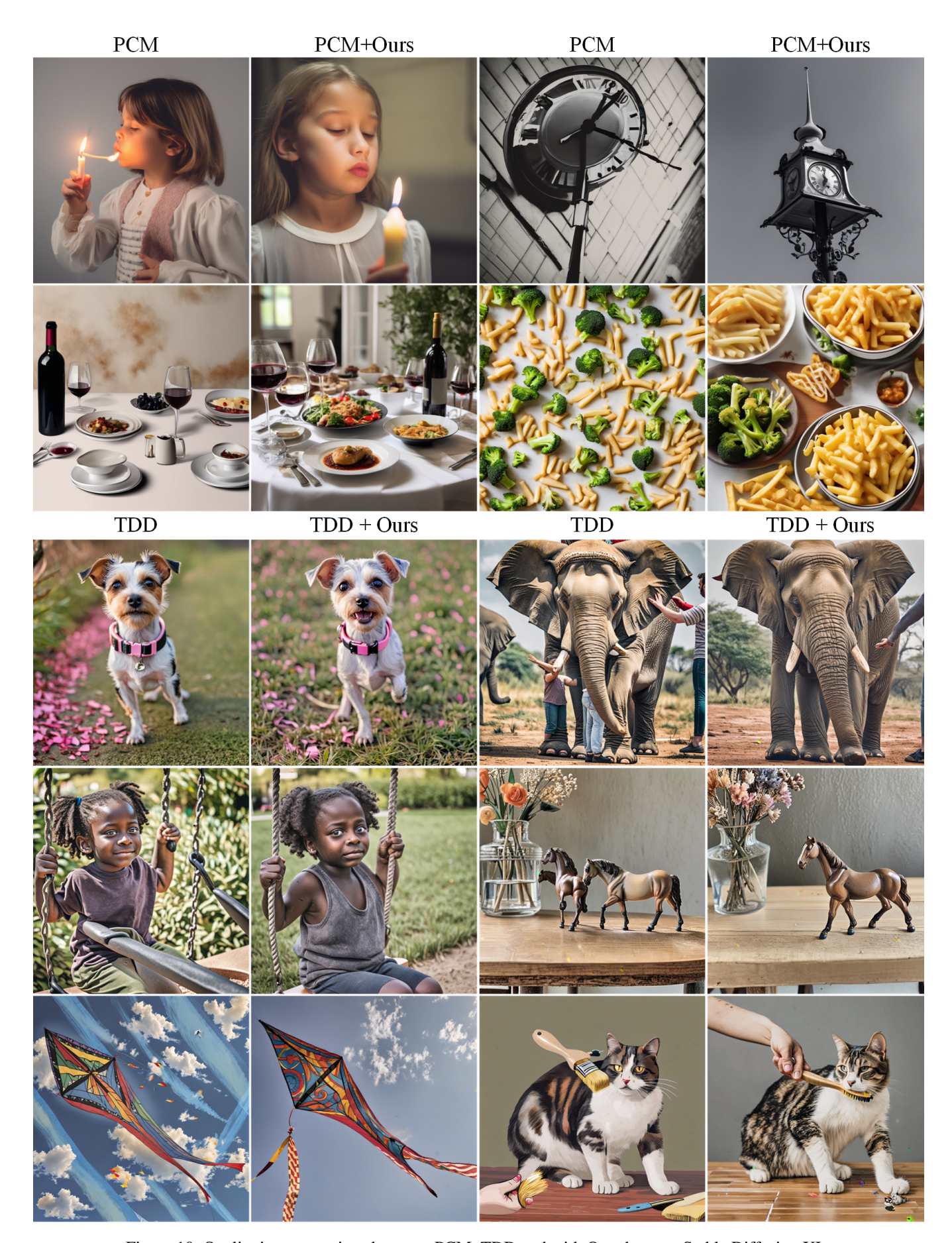


Figure 10: Qualitative comparison between PCM, TDD and with Ours base on Stable Diffusion XL.